INTERNATIONAL JOURNAL OF ADVANCE RESEARCH, IDEAS AND INNOVATIONS IN TECHNOLOGY

ISSN: 2454-132X
Impact Factor: 6.078
(Volume 11, Issue 1 - V11I1-1337)
Available online at: https://www.ijariit.com

Nano-Enhanced Hydrophobic Coating with ZnO Nanoparticles for Preserving Cultural Heritage Building

Dr. Vimal Kumar Jaiswal
vkjasi051104@gmail.com
Archaeological Survey of India, Science Branch, Conservation Research Laboratory, Aurangabad, Maharashtra

Dr. S. Vinodh Kumar
vsvinodhkumar@gmail.com
Archaeological Survey of India, Science Branch, Conservation Research Laboratory, Aurangabad, Maharashtra

Dr. M. K. Bhatnagar
dirspgn-asi@gov.in
Pt. Deendayal Upadhyaya Institute of Archaeology, Archaeological Survey of India, Greater Noida.

ABSTRACT

Preserving outdoor heritage assets is an ongoing challenge in heritage conservation. The purpose of applying preservative coatings is to improve the hydrophobicity of exposed surfaces of building materials and protect against pollutants, microbiological growths, and especially the effects of rainwater. A good protective coating significantly lowers water absorption, maintains high water-vapor permeability, penetrates deeply, is UV light resistant, offers sufficient breathability, and is environmentally friendly. Polysiloxanes and their precursors have been widely used to protect stone surfaces. To avoid degradation or other modifications to the treated surfaces, the treatment's safety and effectiveness must be evaluated before being directly applied to historical materials. In the past, several nanoparticles were developed and tested to improve the functionality of these coatings. The initial protective layer is made of a solvent-based substance called silane-siloxane, which has poor adherence. As a result, water can partially wash off dirt, pollutants, and microbial colonies. The hydrophobicity of protective coating materials made of ZnO nanoparticles is substantially superior. Photocatalytic coatings can oxidize organic materials on surfaces. Pollutant particles and any other dry deposition were quickly and thoroughly removed by rainwater from protective coatings made of nanoparticles.

Keywords: *Stone Protection, Nanostructured Coatings, Nanoparticles, Cultural Heritage Conservation, Hydrophobicity, Photocatalytic Coating, Corrosion, Nobel Metal.*

INTRODUCTION

In material science, nanotechnology is the more innovative and impactable technology. In this technology synthesized the nanometer scale materials which further studied its diverse properties and according to properties applied in various technological applications. Generally, nano means one billionth part of meter or 10^{-9} m. Nanotechnology is a branch of modern technology which comprises the study of materials having dimensions less than 100 nanometres. In 1959, Prof. Richard Feynman at an American Physical Society delivered the lecture entitled, "There's Plenty of Room at the Bottom", this is the birth of nanotechnology. First time in 1974, the term nanotechnology coined by Prof. Norio Taniguchi from Tokyo Science University that describe the mechanism of the materials at atomic-scale level (Sao et al., 2010, Guin et al., 2023). Nanoparticles or nanomaterials are the particles with one or more dimension at nanoscale. Nanoscale materials reveal very drastic change in their properties as compared to its molecule or bulk material. The various properties of the nanoparticles are solely depending upon their phases, sizes, and morphologies etc. Due to the excellent properties such as thermal, electronic, optical, mechanical, catalytic, and magnetic it applied for potential applications such as adsorbents, catalysis, fillers, semiconductors, cosmetics, microelectronics, pharmaceuticals, drug carriers, energy storage and antifriction coatings (Sudha et al., 2018, Haas 2021).

The motion of an electrons consisted in nanomaterials is especially responsible for their physicochemical properties. Mainly the quantum confinement effect is most important in nanometre size materials (Asha et al., 2020). Quantum confinement effect observed in an isolated atom of 1 Å i.e., the size of the particle is comparable to the wavelength of the electron. When the size reduced as comparable to the wavelength of the electron then it can absorb only certain frequency of incident radiation and highly confined to discrete energy levels (Joudeh et al., 2022). In short, due to the reduction of size electrons behave like a wave and it can be hop or tunnel across insulating layers. Thus, size reduction below the 100 nm shows a considerable change in almost all the physicochemical properties as compared to the same bulk materials.

The most recommendable properties of the nanomaterials are surface properties i.e., high surface-to-volume ratio. The high surface to volume ratio of a nanoparticle due to the ~ 90 % of its atom's residence on the surface. Thus, the high surface to volume ratio of nanoparticles proved its potential applications in diverse fields (Roduner 2007).

2. COATING MATERIALS FOR PRESERVATION OF MONUMENTS

Coatings is the best way to protect the historical monuments and cultural heritage (Artesani et al., 2020,Baglioni et al., 2021). Different substances, including different polymers like vinyl acetate copolymers, epoxy, polyurethane, siloxane, alkoxysilanes, fluorinated and acrylic copolymers, have been used as protective coatings, particularly for historical buildings. These coatings decrease the rate of destruction, water penetration, and surface moisture content of porous materials while increasing resistance to atmospheric conditions. The siloxane-based polymers and alkoxysilanes-based nanocomposites have several appropriate properties including good adhesion, high transparency, low surface energy, and good stability (Simionescu et al., 2011, Simionescu et al., 2009). In the present study efficacy of coating materials tested over the brick samples of Laxman temple which is a 7th-century centrally protected monument comes under the jurisdiction of Archaeological survey of India and constructed mostly of brick and this heritage site is located at Sirpur, district Mahasamund in Chhattisgarh state of India.

3. MATERIALS AND METHODS

3.1 Materials

All used chemicals in the present investigation were of highly purified i.e., of AR grade and used as it is any further purifications. A commercial product, consisting of silane-siloxanes (trade mark: SILRES BS-290), SILRES® BS-290, a solvent-less silicone concentrate that is based on a mixture of silane and siloxane products were purchased from Wacker Chemie AG. Zinc chloride ($ZnCl_2$) sodium hydroxide (NaOH) and titanium chloride were purchased from Loba Chem, India.

3.2 Synthesis of Nanoparticles

3.2.1 Synthesis of ZnO nanoparticles

Zinc chloride ($ZnCl_2$) and sodium hydroxide (NaOH) were the starting components used in the chemical co-precipitation process to synthesis ZnO nanoparticles (Ahamed, A. J., 2016). Typically, 100 ml of double-distilled water (DDW) and $ZnCl_2$ (0.4 M) were thoroughly combined in a 200 ml beaker. In a different beaker, a 100 ml solution of sodium hydroxide (0.8 M) was made. Further, NaOH was added to the beaker of $ZnCl_2$ dropwise, and it was agitated for two hours. The resulting milky-white precipitates were filtered using Whatman filter paper and repeatedly washed with DDW. The resulting powder was then calcined in a muffle furnace for two hours at 400 ^{O}C.

3.3 Preparation of hydrophobic coating

A commercial product, consisting of silane-siloxanes (trade mark: SILRES BS-290) diluted with mineral turpentine oil in the ratio of 1:14 as a pure SILRES BS-290 coating. For the nanocomposite with SILERS BS-290 the ZnO nanoparticles was used. Two coating materials were prepared as hydrophobic coating material and tested over the brick samples of Laxman temple.

3.3.1 SILRES BS- 290 + ZnO (2%, 3%, 4%)

The preparation procedure in short, the already prepared ZnO nanoparticles with W/W percentage was dispersed in diluted SILRES BS-290 with mineral turpentine oil ratio of 1:14. In this study the 1% nanoparticles composite not used due to the very small concentration there will be no any significance effect exhibited. The different concentration (2%, 3%, 4%) of ZnO nanoparticles were dispersed in the solution of SILRES BS-290 with harsh stirring and ultra-sonication process.

4. TREATMENTS

Prismatic brick specimens, with dimensions of 5 × 5 × 1 cm^3 and 5 × 5 × 2 cm^3, were cut. According to UNI10921 standard protocol, the samples were smoothened with abrasive paper (180-grit silicon carbide), cleaned with a soft brush, and washed with deionized water in order to remove dust deposits. The stone specimens were completely dried in an oven at 60 ◦C, until the dry weight was achieved, and stored in a desiccator with silica gel (relative humidity (R.H.) = 15%) at 23 ± 2 ◦C. This treatment was performed, on 3 specimens of each dimension, by flooding. Each solution was prepared immediately before use. Three coats of each applied under wet-on-wet condition, until the saturation. The requisite quantity of the coating materials depends on the absorbance capacity of the substrate. In order to allow solvent evaporation and complete condensation, all the treated samples were kept in the laboratory at 25^{0}Cand 45% RH for 30 days and then they were dried in an oven at 60 ^{0}C.

5. CHARACTERIZATION TECHNIQUES

In material science to confirm the materials formation and to check its purity various characterization techniques are developed. For every research which works in the material sciences they should know the detailed information about the characterization techniques. Therefore, we have been discussed here the characterization techniques used in the present investigation**.**

5.1 X-ray Diffraction (XRD)

In the current work, X-ray diffraction (XRD) spectroscopy was used to assess and investigate the structural features of all synthetic materials. One of the most effective and well-known methods for verifying the structural integrity and purity of synthesized materials is X-ray diffractometry (XRD) (Chauhan, A. et. al,2014). Each material researcher utilized XRD to quickly diagnose the structural characteristics of synthesized materials, and based on this, the materials may be used for a variety of purposes. The results of an X-ray diffractogram (XRD) analysis may be used to determine a material's structure, texture, phases, average grain size, strain, crystallinity, and other characteristics. The Bragg's scattering rule found in Equation 5.1, provides the basis for XRD analysis or its fundamental function (Khan, H.,2020).

$$2d \sin\theta = n\lambda - - - - - - - - (5.1)$$

Typically, a monochromatic X-ray beam with a wavelength of between 0.01 – 10 nm is utilised in XRD studies. In the current investigation, an X-ray source called CuK with a wavelength of (1.54 Å) was employed. When the monochromatic X-ray beam attacked the sample, it hindered the dispersion from the samples at various angles in accordance with a set of lattice planes. The originating lattice planes in synthesised materials caused the frustrated scattered rays to produce a unique diffraction pattern. The whole scattering process results in interference patterns, or XRD peaks, that are either constructive or destructive. Structure, Lorenz's factor, polarisation, multiplicity, absorption, temperature, and other factors are also in charge of the relative intensity of the XRD peaks. The peak intensity of XRD patterns obtained by XRD machines solely depends upon the many factors such as stress, strain, temperature, atomic positions, etc. Cation distribution, or the function of X-ray intensity of Bragg's peak, may be determined based on a thorough investigation of the XRD pattern. The primary purpose of an XRD pattern is to reveal the periodic arrangement of atoms inside a crystalline material (Chauhan, A. et al,2014, Khan, H. et al,2020). Regarding the current investigation, certain conducting polymers, nanoparticle composites, and polymer-nanoparticles were synthesised and investigated. According to an X-ray diffractogram (XRD) research, metal oxide nanoparticles have high crystallinity, whereas polymers exhibit poor crystallinity, or amorphous nature.

5.2 Field Emission Scanning Electron Microscopy (FESEM)

The surface morphology has a major influence on the uses of the synthesised materials for sensing applications. Therefore, it is essential to comprehend the approach for surface morphology examination. In order to analyse surface morphology comparison to other microscopes, field emission scanning electron microscopy (FESEM) is a sophisticated technology that is used to see the surface morphology of the prepared sample at higher magnification, better resolution, and depth of focus. Observations of the topography and composition of surfaces, the elemental analysis of materials, internal structure observation, internal characteristic observation, crystalline structure observation, and magnetic domain observation may all be analysed using the FESEM (Pawley, J. B. et. al,1997, Brodusch, N. et. al,2018). The fundamental idea behind FESEM is to bombard the target material with electrons, which then interact with the elements and scatter off of it. Secondary and backscattered electrons are produced by the electrons of the atom scattering. These dispersed electrons provide a picture that contains data about the sample's microstructure. Backscattered electron image and secondary electron image are the two categories under which these pictures fall. Studying surface topography most frequently involves the use of a secondary electron image. Due to the sharp-pointed tip's extremely strong electric field, which is above 107 V/cm, the scanned pictures produced by FESEM give a far higher depth resolution than those produced by conventional microscopes. The electron beam generated by the Field Emission source is around 1000 times smaller than that of a typical microscope using a thermal electron gun, and it may create remarkably high-quality images. Enhanced pictures of the nanomaterials may be seen in FESEM down to atomic size, or around 0.2 nm. When electrons contact with materials in FESEM devices, secondary and backscattered electrons are produced as a result of the atom's electrons scattering. These dispersed electrons provide a picture that contains data about the sample's microstructure. Backscattered electron image and secondary electron image are the two categories under which these pictures fall (Havrdova, M. et. al, 2014).

The Hitachi S-4800 FESEM equipment was utilised in the current experiment to examine the surface morphology of the nanoparticles.

5.3 UV-Visible Spectroscopy

UV-visible (UV-Vis) spectroscopy is used to investigate the optical characteristics of synthesised materials and is based on UV-Vis data. It can also locate the band gap. Functionally, UV-Vis spectroscopy captures how UV-visible light interacts with a substance, either by absorption, transmission, or reflection. The Beer Lambert Law, which forms the foundation of UV-Vis. spectroscopy, asserts that a solution's absorbance is exactly proportional to the concentration of absorbing species in the solution and route length (Förster, H. et.al.,(2004), Perkampus, H. H. et. al., 2013). The Beer Lambert Law is stated mathematically as,

$$I = I_0 e^{-\sigma IN} \text{---------- } 5.3$$

Where, I_0 and $I \rightarrow$ the intensity of the incident and transmitted light,

$\sigma \rightarrow$ the cross-section of light absorption by a single particle and

$N \rightarrow$ the density of absorbing particles

A UV-Vis spectrometer measures the amount of light that goes through a sample (I) and compares it to the amount of light that passes through the sample without passing through it (I_0). Transmittance, commonly represented as a percentage (%T), is the ratio I/I_0. The study of organic molecule impurities and comprehension of the structure of organic substances can both be aided by UV-Vis. spectroscopy.

6. EXPERIMENTAL WORK

Considering the active ingredient as silicone resin and a review of various studies carried out previously showing their suitability as water repellent, it was considered appropriate to carry out laboratory studies with the product at lower concentrations. The following experimental work was carried out in laboratory for comparative evaluation of untreated and treated brick samples of Laxman temple Sirpur.

Measurement of total Water Absorption at 48 hours.

Measurement of water Absorption by Capillarity.

Measurement of water vapour permeability.

6.1 Water absorption at 48 hours

Water absorption by total immersion for 48 hours of untreated sample is a measure of the open porosity of the stone. The results of these tests are shown in table 7.1 as percent (w/w) water absorption for untreated and treated samples after 48 hrs. of total immersion.

6.2 Capillary water absorption

To study the behaviour of protective substances, capillary water uptake measurements were carried out at different time intervals (24 hours). The results show the effect of concentration of active ingredients of Silicone resin in different substrates as the water uptake is reduced corresponding to this concentration. The comparison of water uptake by capillary action between untreated and treated surfaces are given in the table 7.2 Capillary rise rate and weight increase are linear until water reaches the top of the sample.

The capillary protection degree (PDC%) were calculated at these time intervals as follows:

$$PDC\% = \frac{W_{ut} - W_t}{W_{ut}} \times 100 - - - - - - - - - - - (6.2)$$

Wut = Amount of water absorbed by the untreated sample.Wt = Amount of water absorbed by the treated sample at a given time.

6.3 Water vapour Permeability

The water vapour transmission rate mainly depends on the pore radius, hydrophobic effect of the product and its penetration into the substrate. The water vapour permeability rate was calculated using wet cup method by measuring the wet loss every 24 hrs. For measurement of water vapour permeability rate, each stone sample, coated on one side with the preservative was fitted like a plug using silicone sealant into a suitable cup with the little amount of distilled water. The water vapour permeability rate was calculated by measuring the weight loss every 24 hours. This behaviour is particularly important for a stone under hygric condition.

The comparison between water vapour flux before and after each treatment allows us to evaluate the reduction of water vapour permeability.

$$P\% = \frac{W_{ut} - W_t}{W_{ut}} \times 100 - - - - - - - - - (6.3)$$

Wut = Flux of water vapour through the untreated sample.
Wt = Flux of water vapour through the treated sample at a given time.

6.4 SILRES BS-290

6.4.1 Structural Properties of SILRES BS-290

The crystallinity and phase purity of SILRES BS-290 is confirmed via XRD study. Figure 6.1 (a) shows the X-ray diffraction pattern and it exhibits a broad peak at $2\theta = \sim 23^{O}$ with inherent group peak's structure illustrating the amorphous phase.

6.4.2 Optical study of SILRES BS-290 (UV-Vis.)

The optical properties of the SILRES BS-290 coating were analyzed by recording UV-Vis. absorption spectrum in the wavelength range 200-700 nm. Fig.6.1 (b) shows the UV-Vis. absorption spectrum of SILRES BS-290. The maximum absorbance was observed at 225 nm in ultraviolet region which indicates the electronic mechanisms in SILRES BS-290.

6.4.3 Morphological study of SILRESBS-290 (FE-SEM)

The surface morphology of the SILRES BS-290 was picturized by FE-SEM. Fig.6.1(c) shows the FE-SEM image SILRES BS-290. The FE-SEM image clearly envisaged the cauliflower like hydrophobic surface without any crystallinity i.e. amorphous nature.

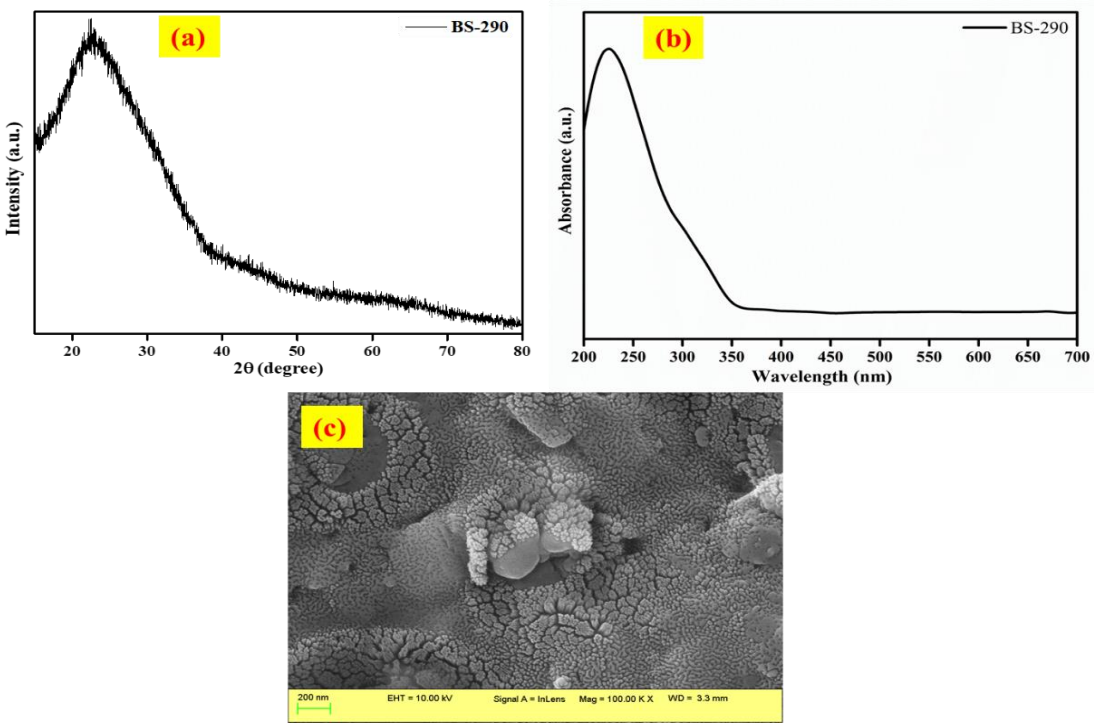

Fig. 6.1 SILRES BS-290 (a) XRD pattern, (b) UV-Vis. absorption spectrum, (c) FE-SEM Micrograph

6.5 Zinc Oxide (ZnO) nanoparticles

6.5.1 Structural and morphological study of ZnO nps

The structural and morphological properties of chemical coprecipitation method synthesized ZnO nanoparticles confirmed by XRD and FESEM characterization techniques. Fig. 6.5(a) shows the XRD pattern of ZnO nanoparticles. The XRD pattern reveals the purity of the synthesized ZnO nanoparticles due to no any unwanted diffraction peak exhibited in the XRD pattern. The diffraction peaks were indexed to the wurtzite hexagonal ZnO (space group P63mc) without any other impurity phases and match with the JCPDS Card No. 96-230-0115. The reflections observed at 32.08^0, 34.82^0, 36.622^0, 48.062^0, 57.182^0, 63.612^0, 67.092^0, 68.722^0, 69.852^0, 73.122^0, 77.862^0 can be indexed to [100], [002], [101], [102], [110], [103], [200], [112], [201], [004], [202] planes of ZnO. The average crystallite size of ZnO nanoparticles is found to be 42.29 nm using Scherer equation

$$D = \frac{0.9\lambda}{\beta \cos\theta} \quad \text{----------(6.5)}$$

No diffracted peaks showing the presence of any impurity is seen which indicates the high purity of the samples synthesized by thermal decomposition route. Fig 6.5(b) shows the FESEM micrograph of the ZnO nanoparticles. The image clearly shows the hexagonal cube of ZnO nanoparticles.

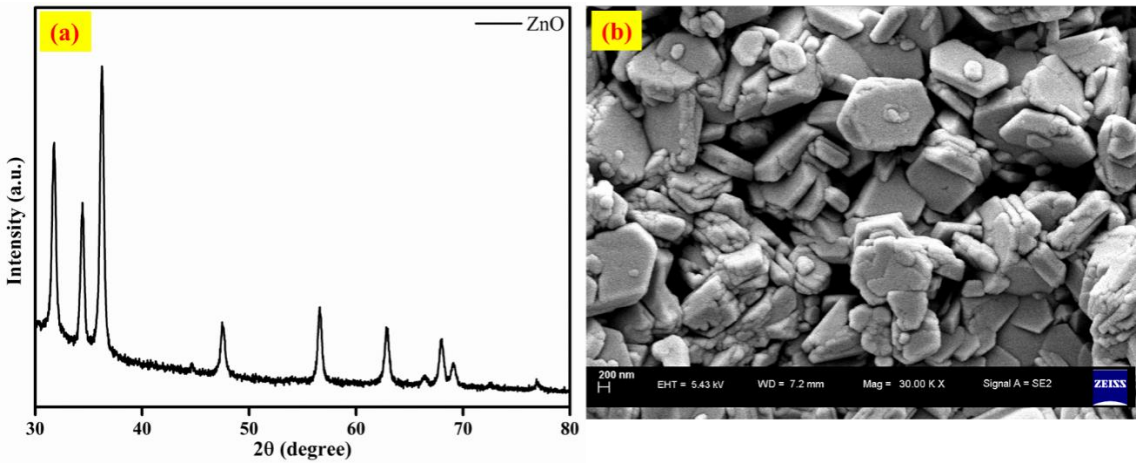

Fig. 6.5 (a) XRD pattern and (b) FESEM image of ZnO nanoparticles

6.6 SILRESBS-290+ ZnO

6.6.1 XRD of BS-290+ ZnO nps

Figure 6.1(a) shows the X-ray diffraction pattern of pure SILRES BS-290 and it exhibits amorphous nature. Fig. 6.6 shows the XRD pattern of SILRESBS- 290+ZnO (2%,3%,4%). When the different concentration of the ZnO nanoparticles incorporated in pure SILRESBS-290 the crystalline peaks originated. The originated peaks are corresponding to the ZnO nanoparticles. At low concertation of ZnO (2%) some ZnO nanoparticles peaks disappears, when increase the concentration (3 %, 4%) all ZnO peaks originated at the proper position of the 2θ value. Thus, the XRD study confirmed the ZnO nanoparticles properly incorporated in the SILRES BS-290.

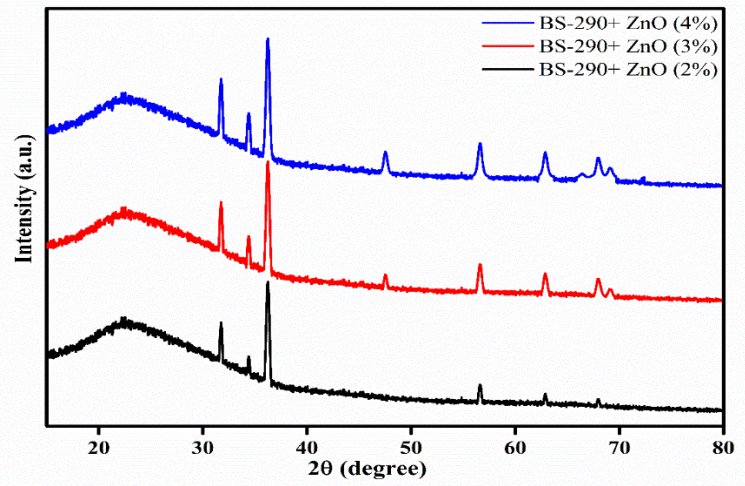

Fig 6.6 XRD Spectrum of BS-290+ZnO (2%,3%,4%)

6.6.2 UV-Vis. study of BS-290+ ZnO

The effects of the incorporation of ZnO nanoparticles on the optical properties of SILRESBS-290 were studied by acquiring UV-Vis. absorptions spectrum. The UV–Vis. spectrum of SILRES BS-290 +ZnO (2%,3%,4%) shown in fig.6.6.2 and it shows the absorbance between 200–300 nm for pureSILRES BS-290.

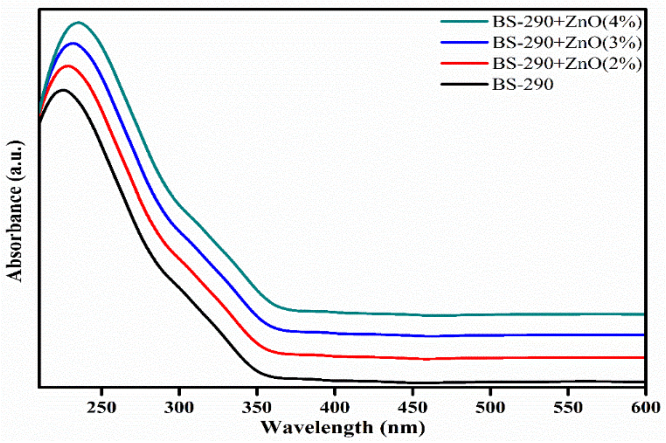

Fig. 6.6.2 UV-Vis. absorption spectrum of SILRES BS-290 +ZnO (2%,3%,4%)

7. COMPARATIVE EVALUATION OF UNTREATED AND TREATED BRICK SAMPLES OF LAXMAN TEMPLE

7.1 Average total water absorption (TWA)

Table 5.1tabulated the experimental results of the average total water absorption (TWA) at 48 hours for three untreated and treated Bricks samples of Laxman temple.

Table 7.1: Total water absorption (TWA) at 48 hours for untreated and treated samples with SILRESBS-290 and BS-290+ZnO

PRODUCT NAME	Laxman temple (TWA) %
Untreated	4.678
BS-290	1.114
BS-290+ ZnO (2 %)	0.944
BS-290+ ZnO (3 %)	0.884
BS-290+ ZnO (4 %)	0.705

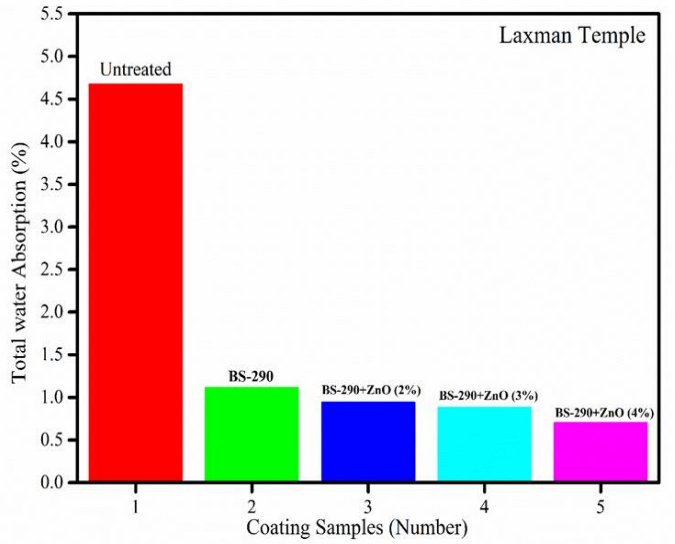

Fig.7.1 Total water absorption (TWA) at 48 hours for Laxman Temple

TWA is measured in percentage before treated and after treated with SILRES BS-290 and BS-290+ZnO. Before treated the TWA shows the value 4.678 %, when treated with BS-290 it decreased and shows 1.114 %. When the coating of BS-290+ZnO applied over bricks sample the value of TWA decreased considerably and lowest value 0.705 % shown for ZnO (4%). The experimental results of water absorption at 48 hours plotted in fig.7.1 and it clearly highlight the coating efficiency of SILRESBS-290+ZnO.

7.2 Capillary water absorption

Table 7.2 shows the Average water capillarity absorption (WCA) measured from 0- 96 hours for three untreated and treated with SILRES BS-290 and BS-290+ZnO (2%, 3%, 4%) of Laxman temple bricks samples. The capillary water absorption for the selected sample measured for from 0-96 hours in the interval of 3 hours. For the quantitative analysis of capillary water absorption, the cumulative inflow per unit area (kg/m^2) against the time is plotted in fig.7.2. Graph shows, the curve consists of a fast increase stage followed by a constant stage due to saturation because of very small capillarity inflow. After treating with SILRESBS-290 and BS-290+ZnO (2%, 3%, 4%) the graph shows the straight line with gradual increment, because of very small capillarity inflow. It clearly evidences that after treating with the SILRES BS-290 and BS-290+ZnO (2%, 3%, 4%)

samples there is very small increment in weight. Therefore, the SILRES BS-290 and BS-290+ZnO (2%, 3%, 4%) are very effective coating for the bricks sample.

Table 7.2: Water capillarity absorption (WCA) at 0- 96 hours for untreated and treated bricks samples with SILRESBS-290 and BS-290+ZnO (2%, 3%,4%)

Average Water Capillarity (Kg/m^2)					
Time	Untreated	BS- 290	BS-290+ ZnO (2%)	BS-290+ ZnO (3%)	BS-290+ ZnO (3%)
0 Hrs	0	0	0	0	0
3 Hrs	1.926	0.094	0.088	0.081	0.07
6 Hrs	3.852	0.187	0.177	0.161	0.141
9 Hrs	5.779	0.281	0.266	0.241	0.211
12 Hrs	5.779	0.374	0.355	0.323	0.281
24 Hrs	5.779	0.748	0.709	0.645	0.561
48 Hrs	5.779	1.502	1.422	1.302	1.123
72 Hrs	5 .779	2.256	2.132	1.945	1.172
96 Hrs	5.779	2.99	2.834	2.586	2.242

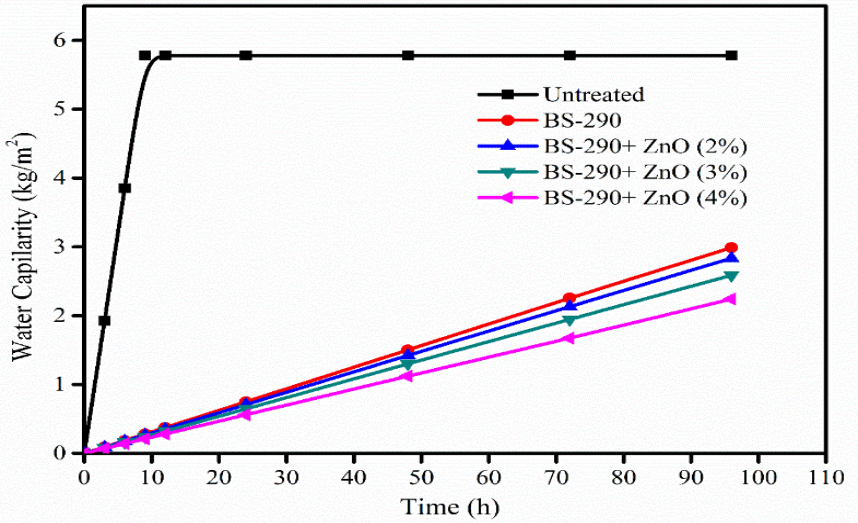

Fig. 7.2Water capillary absorption plots for untreated and treated brick samples

7.3 Water vapour Permeability (WVP):

Average water vapour permeability of the selected bricks samples shown in table 7.3 The experimental value shows that for untreated sample it increases from 7.578-7.889 mg/cm^2/24hrs for 3 to 96 hours. After treating with SILRES BS-290, WVP shows the value from 7.222-7.596 when the ZnO nanoparticles incorporate in BS-290, for ZnO (2%) the value shows in the range of 7.085-7.596, forZnO (3%) 6.905-7.188 and for ZnO(4%) the value shows 6.643-6.975. The rate of the water vapour permeability decreased considerably when ZnO nanoparticles incorporated in BS-290. The experimental values plotted in graph fig.7.3, it shows approximately horizontal straight lines for all samples, but very small increment shown in treated samples.

Table 7.3: Water vapour permeability (WVP) at 3- 96 hours for untreated and treated bricks samples with SILRESBS-290 and BS-290+ZnO (2%, 3%, 4%)

Untreated				
Sr. no	Time (Hrs.)	Wt. of Sample	Water loss	mg/cm^2/24hrs
1	3 Hrs.	103.235	0.009	7.578
2	6 Hrs.	103.238	0.018	7.601
3	9 Hrs.	103.248	0.027	7.675
4	12 Hrs.	103.256	0.037	7.717
5	24 Hrs.	103.275	0.074	7.723
6	48 Hrs.	103.289	0.149	7.756
7	72 Hrs.	103.302	0.224	7.803
8	96 Hrs.	103.367	0.303	7.889

SILRES BS- 290				
Sr. no	Time (Hrs.)	Wt. of Sample	Water loss	mg/cm^2/24hrs
1	3 Hrs.	103.241	0.008	7.222
2	6 Hrs.	103.242	0.017	7.298
3	9 Hrs.	103.246	0.026	7.345
4	12 Hrs.	103.249	0.035	7.404
5	24 Hrs.	103.253	0.071	7.476
6	48 Hrs.	103.276	0.144	7.525
7	72 Hrs.	103.308	0.217	7.55
8	96 Hrs.	103.386	0.292	7.596

SILRESBS- 290 + ZnO (2%)				
Sr. no	Time (Hrs.)	Wt. of Sample	Water loss	mg/cm^2/24hrs
1	3 Hrs.	103.252	0.008	7.085
2	6 Hrs.	103.258	0.017	7.112
3	9 Hrs.	103.256	0.025	7.186
4	12 Hrs.	103.267	0.034	7.207
5	24 Hrs.	103.279	0.069	7.248
6	48 Hrs.	103.29	0.140	7.288
7	72 Hrs.	103.309	0.211	7.342
8	96 Hrs.	103.347	0.284	7.395

SILRES BS- 290 + ZnO (3%)				
Sr. no	Time (Hrs.)	Wt. of Sample	Water loss	mg/cm^2/24hrs
1	3 Hrs.	103.265	0.008	6.905
2	6 Hrs.	103.264	0.016	6.975
3	9 Hrs.	103.271	0.025	7.012
4	12 Hrs.	103.275	0.033	7.055
5	24 Hrs.	103.282	0.068	7.093
6	48 Hrs.	103.301	0.136	7.125
7	72 Hrs.	103.322	0.206	7.168
8	96 Hrs.	103.367	0.276	7.188

SILRESBS- 290 + ZnO (4%)				
Sr. no	Time (Hrs.)	Wt. of Sample	Water loss	mg/cm^2/24hrs
1	3 Hrs.	103.271	0.007	6.643
2	6 Hrs.	103.276	0.016	6.705
3	9 Hrs.	103.282	0.024	6.745
4	12 Hrs.	103.287	0.032	6.798
5	24 Hrs.	103.292	0.065	6.845
6	48 Hrs.	103.314	0.132	6.888
7	72 Hrs.	103.331	0.199	6.903
8	96 Hrs.	103.376	0.268	6.975

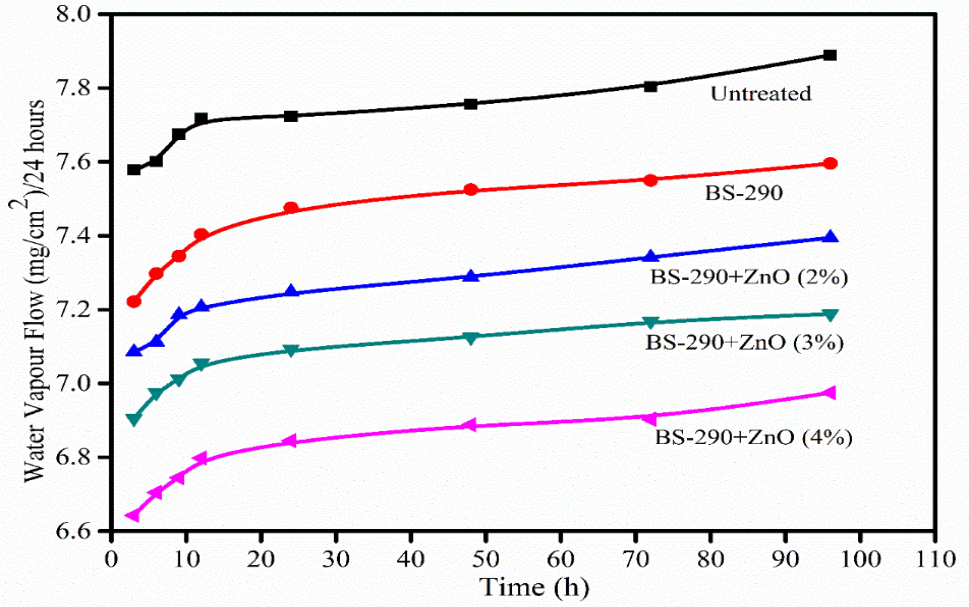

Fig. 7.3 Water vapor permeability curves for untreated and treated brick samples

CONCLUSION

The structural features of the coating materials employed in this study are well described in this study. The XRD examination of the ZnO, nanocomposite revealed appropriate formation with no undesirable impurities. The XRD analysis of pure SILRES® BS-290 proved its amorphous nature. It has also been shown that when ZnO, is added into SILRES® BS-290, the crystallinity rises and the phases of corresponding nanoparticles emerge. UV-Vis. spectroscopy was used to investigate the optical properties of the prepared nanocomposites. The absorption peaks have been discovered in the UV region. The SILRES® BS-290 composite with ZnO, exhibits a red shift in all composites. FESEM images concluded that the ZnO, nanoparticles are well dispersed in SILRES® BS-290.

The SILRES® BS-290 and SILRES® BS-290 nanocomposite BS-290/ZnO (2%, 3% and 4%) has been coated over the brick samples of Laxman temple. Thereafter samples were studied for various water protective properties. The water absorption capacity was measured for 48 hours. It has been observed during analysis that the water absorption value was higher before treating with protective coating while it goes on decreasing when same was treated with SILRES® BS-290 and BS-290+ZnO considerably. This Water capillarity absorption (WCA) has been measured for 96 hours for untreated and treated with SILRES® BS-290 and BS-290+ZnO (2%, 3%, 4%). Before treating with coating, the water capillarity increased up to saturation and thereafter it becomes stable. When coating was done with the SILRES® BS-290 and BS-290+ZnO (2%, 3%, 4%) the capillarity shows constant increment at lower value as compared to untreated sample. Water vapour permeability of samples shows the decrement when treated withSILRES® BS-290 and BS-290+ZnO (2%, 3%, 4%) Thus, the applied coating is compatible for the bricks to protect from water.

9. ACKNOWLEDGEMENT

The author appreciates and acknowledges the opportunity given by the Director General, Archaeological Survey India, New Delhi and the assistance and support of Chemical Conservation Laboratories of Science Branch of Archaeological Survey India. Also, the author acknowledges the guidance of Director (Scientific Preservation), the suggestions and fruitful discussion with Professor Anubhuti Kosle, department of chemistry, Shri Rawatpura Sarkar University, Raipur, Professor Santosh Shrivastav, department of chemistry, CMP College Allahabad. Dr. Prabhakar Undre (Associate Professor) Department of Physics, Dr. Baba Saheb Marathwada University, Aurangabad.

REFERENCES

[1] Sao, P., Nath, D., &Priyadharshini, V. J. (2010). Introduction to Nanoscience and Nanotechnology. AG Publishing House (AGPH Books).

[2] Guin, M., & Singh, N. B. (2023). Nanomaterials: Overview and Historical Perspectives. Emerging Nanomaterials and Their Impact on Society in the 21st Century, 135, 1-22.

[3] Sudha, P. N., Sangeetha, K., Vijayalakshmi, K., &Barhoum, A. (2018). Nanomaterials history, classification, unique properties, production and market. In Emerging applications of nanoparticles and architecture nanostructures (pp. 341-384). Elsevier.

[4] Haas, K. H. (2021). Application of Metal Oxide Nanoparticles and their Economic Impact. Metal Oxide Nanoparticles: Formation, Functional Properties, and Interfaces, 1, 29-65.

[5] Asha, A. B., &Narain, R. (2020). Nanomaterials properties. In Polymer science and nanotechnology (pp. 343-359). Elsevier.

[6] Joudeh, N., &Linke, D. (2022). Nanoparticle classification, physicochemical properties, characterization, and applications: a comprehensive review for biologists. Journal of Nanobiotechnology, 20(1), 262.

[7] Roduner, E. (2007). Nanoscopic materials: size-dependent phenomena. Royal Society of Chemistry.

[8] Ahamed, A. J., & Kumar, P. V. (2016). Synthesis and characterization of ZnO nanoparticles by co-precipitation method at room temperature. Journal of Chemical and Pharmaceutical Research, 8(5), 624-628.

[9] Chauhan, A., & Chauhan, P. (2014). Powder XRD technique and its applications in science and technology. J Anal Bioanal Tech, 5(5), 1-5.

[10] Khan, H., Yerramilli, A. S., D'Oliveira, A., Alford, T. L., Boffito, D. C., & Patience, G. S. (2020). Experimental methods in chemical engineering: X-ray diffraction spectroscopy—XRD. The Canadian journal of chemical engineering, 98(6), 1255-1266.

[11] Pawley, J. B. (1997). The development of field-emission scanning electron microscopy for imaging biological surfaces. Scanning-New York and Baden Baden then Mahwah-, 19, 324-336.

[12] Brodusch, N., Demers, H., & Gauvin, R. (2018). Field emission scanning electron microscopy: New perspectives for materials characterization. Springer Singapore.

[13] Havrdova, M., Polakova, K., Skopalik, J., Vujtek, M., Mokdad, A., Homolkova, M., ...&Zboril, R. (2014). Field emission scanning electron microscopy (FE-SEM) as an approach for nanoparticle detection inside cells. Micron, 67, 149-154.

[14] Förster, H. (2004). UV/vis spectroscopy. Characterization I: -/-, 337-426.

[15] Patil, S. M., Kasthurba, A. K., &Patil, M. V. (2021). Characterization and assessment of stone deterioration on Heritage Buildings. Case Studies in Construction Materials, 15, e00696.

[16] Perkampus, H. H. (2013). UV-VIS Spectroscopy and its Applications. Springer Science & Business Media.

[17] Artesani, A., Di Turo, F., Zucchelli, M., &Traviglia, A. (2020). Recent advances in protective coatings for cultural heritage–an overview. Coatings, 10(3), 217.

[18] Baglioni, M., Poggi, G., Chelazzi, D., &Baglioni, P. (2021). Advanced materials in cultural heritage conservation. Molecules, 26(13), 3967.

[19] Simionescu, B., Olaru, M., Aflori, M., &Doroftei, F. (2011). Siloxane-based polymers as protective coatings against SO2 dry deposition. High Performance Polymers, 23(4), 326-334.

[20] Price, D. G. (1995). Weathering and weathering processes. Quarterly Journal of Engineering Geology and Hydrogeology, 28(3), 243-252.

[21] Srivastava, R. (2012). Synthesis and characterization techniques of nanomaterials. International Journal of Green Nanotechnology, 4(1), 17-27.